Membrane Orientation and Position of the C2 Domain from cPLA2 by Site-Directed Spin Labeling†

April A. Frazier,‡ Mark A. Wisner,§ Nathan J. Malmberg,§ Kenneth G. Victor,‡ Gail E. Fanucci,‡ Eric A. Nalefski,§,|| Joseph J. Falke,*,§ and David S. Cafiso*,‡

Department of Chemistry and Biophysics Program, University of Virginia, Charlottesville, Virginia 22904-4319, and Molecular Biophysics Program and Department of Chemistry and Biochemistry, University of Colorado, Boulder, Colorado 80309-0215

Received December 21, 2001; Revised Manuscript Received March 15, 2002

ABSTRACT: The C2 domain is a ubiquitous Ca^{2+}-binding motif that triggers the membrane docking of many key signaling proteins during intracellular Ca^{2+} signals. Site-directed spin labeling was carried out on the C2 domain of cytosolic phospholipase A_2 in order to determine the depth of penetration and orientation of the domain at the membrane interface. Membrane depth parameters, Φ, were obtained by EPR spectroscopy for a series of selectively spin-labeled C2 domain cysteine mutants, and for spin-labeled lipids and spin-labeled bacteriorhodopsin cysteine mutants. Values of Φ were combined with several other constraints, including the solution NMR structure, to generate a model for the position of the C2 domain at the membrane interface. This modeling yielded an empirical expression for Φ, which for the first time defines its behavior from the bulk aqueous phase to the center of the lipid bilayer. In this model, the backbones of both the first and third Ca^{2+}-binding loops are inserted approximately 10 Å into the bilayer, with residues inserted as deep as 15 Å. The backbone of the second Ca^{2+}-binding loop is positioned near the lipid phosphate, and the two β-sheets of the C2 domain are oriented so that the individual strands make angles of 30−45° with respect to the bilayer surface. Upon membrane docking, spin labels in the Ca^{2+}-binding loops exhibit decreases in local motion, suggesting either changes in tertiary contacts due to protein conformational changes and/or interactions with lipid.

In many cell-signaling pathways, important enzymatic activities and protein−protein interactions take place on the cytoplasmic surface of intracellular membranes. Here diffusion is limited to two dimensions, and the probability of appropriate protein−protein or protein−substrate interactions is enhanced. Regulation in cell-signaling is often achieved by the reversible docking of proteins to the membrane surface, which can be achieved through several mechanisms. One general mechanism involves the electrostatic association of a highly basic protein region with membranes containing acidic lipids, often in tandem with protein acylation (*1*). Another important mechanism utilizes independently folded protein domains that interact with specific membrane interfaces, such as C2 domains (*2*, *3*), or bind individual lipids, such as pleckstrin homology domains (*4*).

The C2 domain was originally identified as the second conserved domain of Ca^{2+}-dependent PKC[1] isoforms (*5*, *6*). This domain generally functions to regulate Ca^{2+}-induced membrane binding, although certain C2 domains mediate protein−protein interactions and some are not regulated by Ca^{2+} at all (*2*, *7*, *8*). A wide range of signaling proteins that are central to the production of lipid-derived second messengers, protein phosphorylation, membrane trafficking, protein ubiquitination, membrane pore formation, and GTPase regulation are found to contain C2 domains (*2*, *9*). Cytosolic phospholipase A_2-α (cPLA2) is a water-soluble lipase with a C2 domain that mediates binding to specific intracellular membranes in a Ca^{2+}-dependent manner (*10*). Upon membrane association, the enzymatic domain hydrolyzes target lipids to release arachidonic acid, triggering the synthesis of eicosanoids that activate various pathways including inflammation (*11*−*13*). High-resolution structures have been obtained for a number of C2 domains including those found in cPLA2, synaptotagmin, protein kinase C, and phospholipase C (*14*−*20*). These structures show that C2 domains are relatively compact and have a common fold consisting of an eight-stranded antiparallel β-sandwich. Three loops at one end of the sandwich play an important role in

† This research was supported by NIH Grants GM62305 (D.S.C.) and GM63235 (J.J.F.).

* Correspondence should be addressed to either of these authors. D.S.C.: Department of Chemistry, University of Virginia, Charlottesville, VA 22904-4319; email: cafiso@virginia.edu. J.J.F.: Department of Chemistry and Biochemistry, University of Colorado, Boulder, CO 80309-0215; email: falke@colorado.edu.

‡ University of Virginia.

§ University of Colorado.

|| Current address: U.S. Genomics, Woburn, MA, 01801.

[1] Abbreviations: bR, bacteriorhodopsin; cPLA2, cytosolic phospholipase A_2-α; dPE, dansyl-phosphatidylcholine; DPPH, α,α′-diphenyl-β-picrylhydrazyl; EPR, electron paramagnetic resonance spectroscopy; FRET, fluorescence resonance energy transfer; HEPES, *N*-(2-hydroxyethyl)piperazine-*N*′-2-ethanesulfonic acid; K_B, reciprocal molar membrane binding constant; LUV, large unilamellar vesicle; MTSSL, methanethiosulfonate spin label; NiEDDA, nickel(II) ethylenediaminediaacetic acid; O_2, oxygen; PIPES, piperazine-*N*,*N*′-bis(2-ethanesulfonic acid); PKC, protein kinase C; PLC, phospholipase C; PC, phosphatidylcholine; POPC, palmitoyloleoylphosphatidylcholine; POPS, palmitoyloleoylphosphatidylserine; PS, phosphatidylserine; SUV, small unilamellar vesicle.

10.1021/bi0160821 CCC: $22.00
Published on Web 04/24/2002

Scheme 1

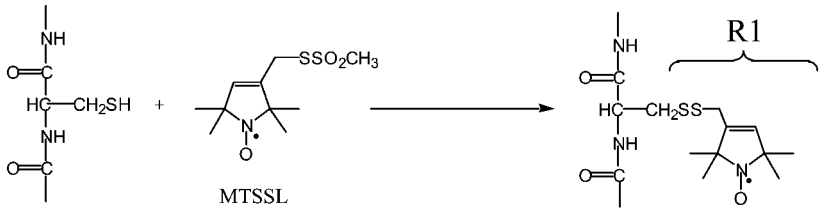

calcium and membrane binding (*17*, *21*−*23*). The X-ray crystal structure of the full-length cPLA2 enzyme reveals that the C2 domain and enzymatic domains are separated by a flexible linker and are structurally independent (*24*). Further biochemical studies have found that the isolated C2 domain retains the ability to bind membranes in a Ca^{2+}-dependent fashion (*25*), justifying structural and mechanistic studies of the isolated domain.

At least four major factors are believed to drive the membrane docking of C2 domains (*2*): (i) favorable, direct contacts between protein surface residues, including the bound Ca^{2+} ions, and phospholipid headgroups (*26*); (ii) favorable long-range electrostatic interactions between the protein−Ca^{2+} complex and the membrane (*3*, *18*, *27*); (iii) hydrophobic interaction of surface-exposed apolar residues with the membrane interior (*3*, *25*, *27*); and (iv) entropically favored release of bound water from the protein−membrane interface upon C2 domain binding. The relative contributions of these components are known to differ dramatically between C2 domains. For example, the C2 domain of PKC-β and the first C2 domain of synaptotagmin I each require the presence of acidic lipid and exhibit ionic strength-sensitive docking, whereas the cPLA2 C2 domain prefers membranes composed of zwitterionic PC and is not dependent on ionic strength (*3*, *27*). To determine the likely contributions of different binding forces, a higher resolution picture of the protein−membrane interface is essential. Structural characterization of this interface is also a prerequisite for understanding how Ca^{2+} binding to the C2 domain triggers membrane docking.

Currently, the structural information available for the C2 domain−membrane interface is limited, and there are inconsistencies among the data. From photolabeling and monolayer experiments, the cPLA2 C2 domain appears to penetrate the membrane (*23*, *27*, *28*). Fluorescence data place all three Ca^{2+}-binding loops in contact with the membrane, while the β-strands exhibit no direct membrane contacts (*21*). A model generated in a previous EPR study places Ca^{2+}-binding loop 3 into the bilayer, loop 1 on the aqueous side of the lipid phosphates, and β-strand 3 close to the interface (*22*). One difficulty with the fluorescence study is that it mapped out the protein surface that interacts with the membrane but did not quantitate distances. In contrast, the EPR study measured distances from the membrane surface to water-exposed residues but did not quantitate the depth of penetration into the bilayer. Moreover, the EPR measurements used lower ionic strength and vesicles composed of a charged nonphysiological acidic lipid, conditions which may have perturbed the docking interaction. NMR chemical shift changes that were measured in detergent micelles provide an indication of the protein surfaces that contact membranes (*17*). Surprisingly, chemical shift changes at regions distal to the putative binding face were also observed. Such studies are complicated by the fact that micelle systems are not the best model for the membrane interface.

In the present study, site-directed spin labeling (*29*, *30*) together with the known solution structure of the cPLA2 C2 domain (*17*) were used to develop a new model for the depth of penetration and orientation of the C2 domain at the membrane interface. Specifically, a series of single cysteine substituted mutants of this domain were reacted with the sulfhydryl-reactive methanethiosulfonate spin label (MTSSL) to produce the spin-labeled side chain R1 (Scheme 1).

The EPR spectra of these mutants were power-saturated in the presence of an aqueous metal ion complex or lipid-soluble oxygen, and the data were used to determine the label position relative to the lipid phosphate using a collision gradient method described previously (*31*). The data are shown to be consistent with an orientation where the first and third Ca^{2+}-binding loops penetrate significantly into the bilayer interior, while the backbone of the second Ca^{2+}-binding loop contacts the membrane surface. No contacts are detected between the β-strands and the membrane. The EPR line shapes also provide evidence for interactions with immobilized lipid or conformational changes upon membrane association. Finally, the EPR data, together with the known C2 domain structure, define for the first time the shape of the distance dependence for the EPR membrane depth parameter in the aqueous region just outside the membrane.

MATERIALS AND METHODS

Materials. Palmitoyloleoylphosphatidylcholine (POPC), palmitoyloleoylphosphatidylserine (POPS), 5-, 7-, 10-, and 12-doxyl spin-labeled phosphatidylcholines were purchased from Avanti Polar Lipids (Birmingham, AL) and used without further purification. Dansyl-PE [*N*-(5-dimethylaminonaphthalene-1-sulfonyl)-1,2-dihexadecanoyl-*sn*-glycero-3-phosphoethanolamine] was obtained from Molecular Probes (Eugene, OR), and the sulfhydryl-reactive spin label 1-oxyl-2,2,5,5-tetramethyl-Δ^3-pyrroline-3-methyl methanethiosulfonate (MTSSL) was purchased from Toronto Research Chemicals, Inc. (North Fork, Ontario, Canada). The paramagnetic reagent nickel(II) ethylenediamine-*N*,*N*′-diaacetic acid (NiEDDA) was synthesized as described previously (*31*). Unfolded, lyophilized bacterio-opsin cysteine mutants in SDS detergent were generously provided by Duncan Greenhalgh and Gobind Khorana. The mutants were refolded, regenerated, and reconstituted as previously described (*32*) into a lipid mixture of 3:1 POPC/POPS.

Preparation, Purification, and Spin Labeling of Single Cysteine Mutants. Site-directed mutagenesis to produce single cysteine mutants of the C2 domain from cytosolic phospholipase A_2-α was carried out as described previously (*21*, *25*). Native and single cysteine mutated C2 domains were expressed in *E. coli*, refolded from inclusion bodies,

and affinity-purified on a phosphatidylcholine (PC) matrix (*25*). The domain was spin-labeled by reacting the cysteine-containing protein with a 3-fold molar excess of MTSSL in the dark for 30 min (*33*). The resulting labeled protein was separated from unreacted label by repetitive dilution and ultrafiltration.

Measurement of C2 Domain Membrane Affinities. The affinities of the spin-labeled C2 domain for POPC/POPS membranes were measured as previously described (*3*, *34*). In these measurements, FRET was used to monitor the proximity of a protein-bound donor (intrinsic Trp 71) to a membrane-bound acceptor (dansyl-phosphatidylethanolamine, or dPE). Small unilamellar vesicles (SUVs) composed of 3:1 POPC/POPS and 5% dPE were prepared in 100 mM KCl, 20 mM HEPES, pH 7.4, by sonication. The SUVs were titrated into a solution containing 0.5 μM C2 domain and 1 mM $CaCl_2$ in the same buffer, yielding a total lipid concentration ranging from 1 to 300 μM. At 25 °C, protein-to-membrane FRET was monitored by exciting the donor ($\lambda_{ex} = 284$ nm) while measuring the acceptor emission ($\lambda_{em} = 520$ nm). The FRET signal increases with the concentration of acceptor-containing vesicles (POPC/POPS, 3:1, containing 5% dPE) as the C2 domain docks to the membrane, until saturation is achieved. A binding constant, K_B, and the standard deviation were determined by nonlinear least-squares best-fit of a standard binding equation for a homogeneous population of independent binding sites. The lipid affinity of each mutant relative to wild type was calculated as the ratio K_B(mutant)/K_B(wild type) for mutant and wild-type data measured in parallel, and the error of the relative affinity was propagated from the best-fit errors for the numerator and denominator.

Large Unilamellar Vesicles for EPR. Large unilamellar vesicles (LUVs) were prepared with a POPC:POPS ratio of 3:1 by mixing the appropriate aliquots of lipids, drying the solution under a stream of argon, and vacuum-desiccating the mixture overnight. The resulting film was hydrated in a buffer of 1 mM $CaCl_2$, 100 mM KCl, 20 mM PIPES, pH 7.0, for 1 h, vortexed thoroughly, and extruded through a polycarbonate filter with a 0.1 μm pore diameter using a hand-held Mini-Extruder (Avanti Polar Lipids, Birmingham, AL). Lipids were extruded at a total concentration of approximately 150 mM and then diluted for use. For measurements of the spin-labeled lipid standards, doxyl 5-, 7-, 10-, and 12-PCs at a concentration of approximately 1 mol % were codissolved in chloroform with POPC/POPS (3:1) and extruded to form LUVs as described above.

EPR Measurements. For EPR spectroscopy, protein sample concentrations typically ranged from 20 to 200 μM, and the lipid vesicles (LUVs) were used at a concentration of 37 mM or higher to ensure complete membrane binding and low surface densities. Buffer solutions contained 1 mM $CaCl_2$, 100 mM KCl, 20 mM PIPES, pH 7.0, except for measurements made under conditions of high-viscosity which also contained 30% Ficoll 400. EPR spectra were recorded using either a Bruker ESP300 spectrometer or a Varian E-line Centuries series spectrometer. Both were fitted with X-band loop-gap resonators (Medical Advances, Milwaukee, WI). All full spectra were recorded at room temperature and were typically an average of two, 4-min scans. From the peak-to-peak line width of the EPR central resonance, δ, the scaled mobility, M_s, for the nitroxide was determined from: $M_s = (\delta^{-1} - \delta_i^{-1})/(\delta_m^{-1} - \delta_i^{-1})$. Here δ_m and δ_i represent the line widths of the most mobile and immobile MTSSL labels previously observed in proteins (*30*).

Continuous-wave power saturation measurements were performed by placing samples in gas-permeable TPX capillaries (Medical Advances, Milwaukee, WI) and recording the peak-to-peak first-derivative amplitude, A_{pp}, of the $m_I = 0$ resonance as a function of microwave power, P. A_{pp} was then fit to the expression:

$$A_{pp}(0) = I\sqrt{P}\left[1 + (2^{\epsilon} - 1)\frac{P}{P_{1/2}}\right]^{-\epsilon} \quad (1)$$

where I is a scaling factor, $P_{1/2}$ is the microwave power required to reduce the resonance amplitude to half of its unsaturated value, and ϵ is a measure of the homogeneity of the saturation of the resonance (*31*). In this fit, I, ϵ, and $P_{1/2}$ are adjustable parameters and yield a characteristic $P_{1/2}$. Values for $P_{1/2}$ are then generated for each sample under three different conditions: (1) equilibrated with nitrogen; (2) equilibrated with air (20% oxygen); and (3) equilibrated with nitrogen in the presence of NiEDDA (experimental concentrations ranged from 10 to 100 mM NiEDDA, but were normalized to an effective concentration of 20 mM). From these values of $P_{1/2}$, a collision parameter for O_2 (Π^{oxy}) was determined according to

$$\Pi^{oxy} \equiv \frac{\Delta P'_{1/2}(O_2)}{P'_{1/2}(DPPH)} = \frac{P_{1/2}(O_2)/\Delta H_{pp}(O_2) - P_{1/2}(N_2)/\Delta H_{pp}(N_2)}{P_{1/2}(DPPH)/\Delta H_{pp}(DPPH)} \quad (2)$$

Here, ΔH_{pp} is the peak-to-peak line width for the central resonance of the EPR spectra. A similar expression can be written for Π^{NiEDDA}, the collision parameter for NiEDDA. $P_{1/2}$(DPPH) and ΔH_{pp}(DPPH) were obtained for a solid sample of DPPH (α,α′-diphenyl-β-picrylhydrazyl) (*35*). A depth parameter, Φ, was calculated from the Π values by the expression:

$$\Phi = \ln\left[\frac{\Pi^{oxy}}{\Pi^{NiEDDA}}\right] \quad (3)$$

Reference points for Φ values at known positions within the bilayer were obtained for doxyl-labeled phosphatidylcholines and bacteriorhodopsin (bR) mutants in membranes having the same lipid composition as that used for power saturation measurements on spin-labeled cPLA2 C2 domain. The positions of the spin-labeled lipids and bR mutants were taken to be those published previously (*31*, *36*).

Modeling the Orientation of the C2 Domain. Previous work has shown that there is a roughly linear dependence of Φ as a function of depth within the bilayer interior for both protein- and lipid-associated spin labels (*31*). However, this relationship fails at distances that are sufficiently far from the membrane interface because the standard-state chemical potentials of oxygen and metal complex approach their bulk values. Since many sites on the C2 domain are expected to lie near but outside the membrane interface, a behavior for Φ on the aqueous side of the bilayer interface is needed. The value of Φ must become distance-independent in bulk

solution (or in bulk hydrocarbon) but have a continuous transition to a more linear region within the membrane interior. The expected behavior may be described by a hyperbolic tangent function:

$$\Phi = A \tanh[B(x - C)] + D \quad (4)$$

where x represents the distance of the label from the lipid phosphate (positive values of x are inside and negative values are outside the bilayer), A and D set the bulk values of Φ in water and hydrocarbon, C determines the position of the reflection point of the curve, and B determines the slope of the curve. On the aqueous side of the membrane interface, eq 4 asymptotically approaches a minimum value associated with the bulk aqueous phase. Inside the bilayer, eq 4 increases approximately linearly but eventually approaches a maximum limiting value. As shown below (see Results), this function accurately describes previously published data.

To model the orientation and position of the C2 domain at the membrane interface, the R1 side chain was appended to the NMR-derived structure of the cPLA2 C2 domain (PDB ID: 1BCI) (*17*) at the labeled sites. The modeling and distance computations were carried out using WebLab ViewerPro (MSI, Inc., San Diego, CA), Insight (MSI, Inc.), and MatLab (The Mathworks, Natick, MA). Most of the labels were placed in configurations determined by recent crystallographic studies on R1 (*37*), where the first and second dihedral angles are in a $g+g+$ conformation. Residues 59, 64, and 106 were placed in a $g+t$ configuration due to steric constraints. A set of coordinates for the nitrogen atom on the R1 side chain was then generated, and the membrane-bound position of the C2 domain was defined by three Euler angles and its placement along the bilayer normal. The position of the domain was varied along with the quantities (D − A), B, and C of eq 4 to find the best-fit between the C2 domain data, the spin-labeled phosphatidylcholine and bacteriorhodopsin calibration points, and the form of eq 4. Thus, seven parameters were simultaneously varied to generate a self-consistent model describing both the depth-dependence of Φ and the location of the C2 domain in the membrane. The resulting model is constrained by the form of eq 4, Φ data for the C2 domain, Φ values for spin-labeled lipids and bR, and geometrical constraints imposed by the solution structure of the C2 domain.

RESULTS

Labeling and Membrane Binding of Mutant C2 Domains. Thirteen single-cysteine mutants of the cPLA2 C2 domain were labeled with MTSSL and purified. A fluorescence resonance energy transfer (FRET) assay (see Materials and Methods) was used to determine the effect of each cysteine mutation and each R1-derivatized mutant on the C2 domain affinity for POPC/POPS membranes. Shown in Figure 1 are representative binding curves for two C2 domain mutants, and Table 1 summarizes the membrane affinity, relative to wild type, of each unlabeled and spin-labeled mutant. For comparison, previously measured relative affinities for these same mutants derivatized with 5-fluorescein-maleimide (5-FM) are also shown. In general, the introduction of a cysteine or R1 side chain has little effect on membrane docking. Cysteine mutations outside the calcium-binding loops yield lipid affinities within a factor of 2 of wild type, and the effects of R1 at these sites are negligible. Two cysteine mutations within the calcium-binding loops are more perturbing: the replacement of an aromatic residue with cysteine at position 35 in calcium-binding loop 1, or at position 96 in calcium-binding loop 3, results in a dramatic decrease in membrane affinity. However, incorporation of the R1 side chain at these sites recovers much of the lipid affinity, restoring the binding constants to within 2-fold of the wild-

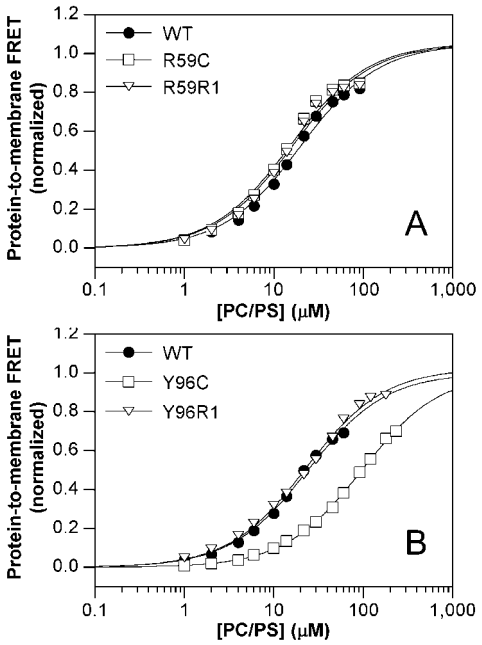

FIGURE 1: FRET measurements of membrane affinity. A FRET assay was used to monitor the proximity of a protein fluorescence donor (intrinsic Trp 71 of the C2 domain) to a membrane-bound acceptor (dansyl-labeled phosphatidylethanolamine, or dPE) (see Materials and Methods). The solid lines are best-fit curves calculated for homogeneous binding sites. Experiments were conducted at 25 °C in a buffer containing 100 mM KCl, 20 mM HEPES, 1 mM $CaCl_2$, pH 7.4.

Table 1: Membrane Affinities of Modified cPLA2 C2 Domain Relative to Wild Type[a]

mutation	location[b]	cysteine mutant	R1 labeled	5-FM labeled
F35C	β1-β2 (CBL1)	0.19 ± 0.02	0.6 ± 0.1	0.4 ± 0.2
L39C	β1-β2 (CBL1)	0.57 ± 0.07	1.4 ± 0.2	0.3 ± 0.1
S51C	β2	1.1 ± 0.3	1.0 ± 0.2	2 ± 1
R59C	β3	1.3 ± 0.3	1.2 ± 0.3	0.8 ± 0.5
N64C	β3-β4 (CBL2)	0.9 ± 0.2	0.17 ± 0.03[c]	1.3 ± 0.5
N68C	β3-β4 (CBL2)	1.2 ± 0.3	0.7 ± 0.1	1.8 ± 0.6
N72C	β4	0.9 ± 0.2	0.9 ± 0.3	1.0 ± 0.7
N82C	β4-β5	0.7 ± 0.2	0.7 ± 0.2	1.3 ± 0.8
Y96C	β5-β6 (CBL3)	0.18 ± 0.03	0.8 ± 0.1	0.2 ± 0.1
M98C	β5-β6 (CBL3)	0.7 ± 0.2	0.8 ± 0.3	5 ± 2
T106C	β6	1.0 ± 0.3	1.2 ± 0.4	0.5 ± 0.2
K113C	β6-β7	1.2 ± 0.3	1.0 ± 0.2	1.1 ± 0.4
N125C	β7-β8	1.0 ± 0.3	0.7 ± 0.1	1.0 ± 0.3

[a] A FRET assay was employed to measure the lipid affinity of each modified protein (see Materials and Methods). The affinities compare cysteine mutants, R1-labeled mutants, and 5-fluorescein-maleimide (5-FM)-labeled cysteine mutants (*21*) to wild type: K_B(mutant)/K_B(WT). For wild type, the average binding constant was $K_B = (6 \pm 2) \times 10^4$ M^{-1}, corresponding to a dissociation constant of $K_D = 16 \pm 4$ μM. [b] Positions located on calcium- and membrane-binding loops are indicated CBL, and those on β-strands or non-calcium-binding loops between strands are indicated by the strand number. [c] Of the R1-labeled mutants, only N64R1 exhibited a membrane affinity change over 2-fold.

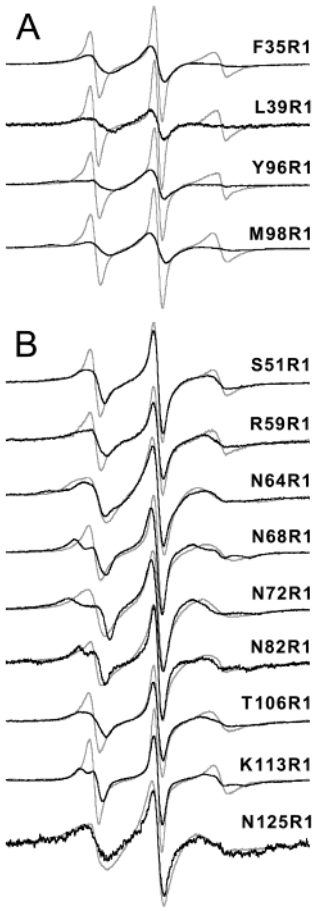

FIGURE 2: X-band EPR spectra of spin-labeled C2 domain mutants in the absence (shaded line) and presence (solid line) of PC/PS (3:1) lipid vesicles. All EPR spectra were recorded with a lipid to protein ratio of 200:1 or greater in a buffer containing 1 mM $CaCl_2$, 100 mM KCl, 20 mM PIPES, pH 7.0, at 25 °C, and have been normalized against the total number of spins. The amplitudes for pairs of mutant spectra have been scaled independently.

type protein. Of the spin-labeled mutants, only N64R1 in the second Ca^{2+}-binding loop alters the lipid affinity at least 2-fold compared to the wild-type protein. Overall, Table 1 shows that the smaller R1 side chain is less disruptive than the larger 5-FM probe. In particular, labeling with 5-FM alters the lipid affinity more than 2-fold at 6 of the 13 positions tested. The remarkably small effects of R1 on lipid affinity as well as the observation that R1 generally does not perturb protein structure (*33*) are consistent with the fact that R1 is similar in size and hydrophobicity to some natural side chains.

EPR Spectra Reveal Binding to POPC/POPS Membranes. EPR spectra for 13 spin-labeled C2 domain mutants are shown in Figure 2 in the absence and presence of POPC/POPS (3:1) membranes. All samples included 1 mM Ca^{2+} to ensure full occupancy of the C2 domain Ca^{2+}-binding sites. In addition, the 37 mM average lipid concentration and 200:1 lipid to protein molar ratio ensured that all modified proteins were completely membrane-associated at low surface density. For every spin label position, membrane association causes the EPR spectrum to broaden and decrease in amplitude, suggesting a loss of C2 domain rotational diffusion on the nanosecond time scale upon membrane docking. Spin label positions 35, 39, 96, and 98 (Figure 2A) yield the most dramatic amplitude losses upon membrane

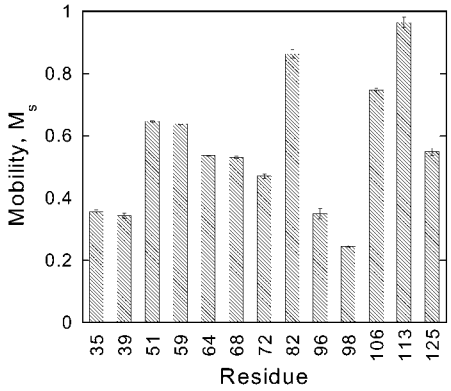

FIGURE 3: Scaled mobilities, M_s, for R1 side chains attached to the C2 domain when fully bound to PC/PS (3:1) membranes. Maximal values of M_s are obtained for labels in loop regions opposite the membrane-binding face (positions 82 and 113); minimal values are obtained for labels in loop regions associated with the membrane (positions 35, 39, 96, and 98). Error bars were generated by best-fit estimates of the line width.

association. Each of the membrane-bound spectra shown in Figure 2 is consistent with surface-labeled sites. At several positions, for example, 68, 72, 82, and 113, the spectra are similar to others seen at sites where there is a single dynamic population undergoing anisotropic motion (*38*). To compare the spin label rotational dynamics of different labeling positions in the membrane-docked state, the line width of each membrane-associated spectrum was used to calculate a scaled R1 side chain mobility (M_s), summarized in Figure 3 (see Materials and Methods). These mobilities provide an approximate measure of label dynamics ranging from $M_s = 1$ for the most mobile R1 side chains in proteins to $M_s = 0$ for the most immobile R1 side chains (*30*). The largest R1 side chain mobilities are found at positions 82 and 113 located in loop regions at the end of the domain distal to the membrane docking face. The M_s values at these positions are consistent with values observed in the loop regions of proteins and indicate that these distal loops are very dynamic even in the membrane-docked state. The lowest M_s values are found at positions 35, 39, 96, and 98 in the first and third calcium-binding loops. These loops are on the membrane-interacting face of the domain, and the lower mobility at these sites may reflect either diminished backbone motion of the loops or restricted local rotation of the labeled side chains due to interactions with phospholipids. Thus, for the membrane-bound C2 domain, the EPR line widths indicate that side-chain labels on the water-exposed loops are highly dynamic whereas labels at the membrane interface undergo significantly less motional averaging.

Collision Parameters Indicate That Two Ca^{2+}-Binding Loops Penetrate into the Membrane. Each of the spin-labeled mutants shown in Table 1 was power-saturated to determine collision parameters between the R1 side chain and either O_2 or NiEDDA as described under Materials and Methods. In these experiments, lipid-soluble O_2 serves as a probe for membrane insertion, while the polar NiEDDA tests for aqueous exposure. Table 2 summarizes the collision parameters Π^{oxy} and Π^{NiEDDA} for each of the mutants, as well as for spin-labeled lipids and bR mutants incorporated into PC/PS (3:1) vesicles. Figure 4 plots Π^{oxy} versus Π^{NiEDDA}, and also displays the previously determined boundaries that define the R1 label environment (*39*). Data are shown for

Table 2: Collision and Depth Parameters for cPLA2 C2 Domain, Lipid, and Bacteriorhodopsin Associated Spin Labels[a]

mutant	Π^{oxy}_{aq}	Π^{NiEDDA}_{aq}	Π^{oxy}_{lipid}	Π^{NiEDDA}_{lipid}	Φ_{lipid}	distance[c]	distance[d]
F35C	0.15 ± 0.01	1.46 ± 0.06	0.34 ± 0.03	0.08 ± 0.01	1.45 ± 0.15	9.1	9.4
L39C	0.43 ± 0.02	5.52 ± 0.27	0.46 ± 0.03	0.02 ± 0.01	3.14 ± 0.50	14.8	14.7
S51C	0.23 ± 0.01	2.52 ± 0.11	0.17 ± 0.01	1.90 ± 0.06	−2.41 ± 0.07	−4.8	(−11.5)
R59C	0.19 ± 0.01	3.15 ± 0.11	0.11 ± 0.01	1.08 ± 0.06	−2.28 ± 0.11	0.4	(−7.4)
N64C	0.19 ± 0.01	1.11 ± 0.06	0.11 ± 0.01	0.52 ± 0.03	−1.55 ± 0.11	2.6	−0.2
N68C	0.22 ± 0.01	1.97 ± 0.10	0.14 ± 0.01	1.12 ± 0.04	−2.08 ± 0.08	−15.4	(−4.3)
N72C	0.24 ± 0.01	2.24 ± 0.09	0.18 ± 0.02	2.35 ± 0.09	−2.57 ± 0.12	−21.9	nd
N82C	0.38 ± 0.02	4.44 ± 0.19	0.25 ± 0.01	2.05 ± 0.15	−2.10 ± 0.09	−17.9	(−4.5)
Y96C	0.40 ± 0.02	5.29 ± 0.21	0.29 ± 0.02	0.16 ± 0.02	0.59 ± 0.14	5.5	7.1
M98C	0.25 ± 0.01	2.42 ± 0.08	0.27 ± 0.03	0.08 ± 0.03	1.22 ± 0.39	7.7	8.8
T106C	0.17 ± 0.02	1.50 ± 0.11	0.16 ± 0.02	1.35 ± 0.08	−2.13 ± 0.14	−4.4	(−4.9)
K113C	nd[b]	nd	0.20 ± 0.02	1.59 ± 0.06	−2.07 ± 0.11	−30.6	(−4.2)
N125C	0.21 ± 0.02	3.72 ± 0.26	0.21 ± 0.02	1.82 ± 0.33	−2.16 ± 0.20	−4.4	(−5.3)
5-DOXYL			0.31 ± 0.02	0.07 ± 0.01	1.49 ± 0.15	8.1	9.5
7-DOXYL			0.39 ± 0.03	0.05 ± 0.01	2.05 ± 0.21	10.5	11.0
10-DOXYL			0.56 ± 0.04	0.05 ± 0.01	2.42 ± 0.21	14.0	12.1
12-DOXYL			0.67 ± 0.04	0.04 ± 0.01	2.82 ± 0.26	16.0	13.4
bR 109			0.44 ± 0.05	0.05 ± 0.01	2.17 ± 0.23	11.0	11.4
bR 116			0.61 ± 0.06	0.01 ± 0.007	4.11 ± 0.71	20.5	21.1
bR 117			0.67 ± 0.06	0.01 ± 0.006	4.20 ± 0.61	22.5	22.3
bR 124			0.21 ± 0.03	0.03 ± 0.01	1.95 ± 0.36	10.5	10.7

[a] All membrane-associated spin labels were measured in membranes having identical compositions using the same paramagnetic reagents. Collision data for the cPLA2 C2 domain are given with no lipid present (aq) and bound to PC/PS LUVs (lipid). [b] Not determined (nd). [c] Distances for the C2 domain spin labels were obtained from the model shown in Figure 6 and correspond to the position of the nitrogen atom on R1 in angstroms from the plane of the lipid phosphates. Positive distances are within the bilayer whereas negative distances are in the aqueous phase. The uncertainty in these distances, as defined by the uncertainty in Φ and constrained by the structural model, is on the order of ±3 Å. This error corresponds to an uncertainty in the Euler angles defining the C2 domain orientation of about ±5°. [d] Theoretical distances were calculated from Φ using eq 4. Parentheses indicate values of $\Phi < -2.0$, which are obtained for sites lying in the aqueous phase a few angstroms from the membrane. For these sites, distances are poorly determined as indicated by eq 4 and Figure 5B.

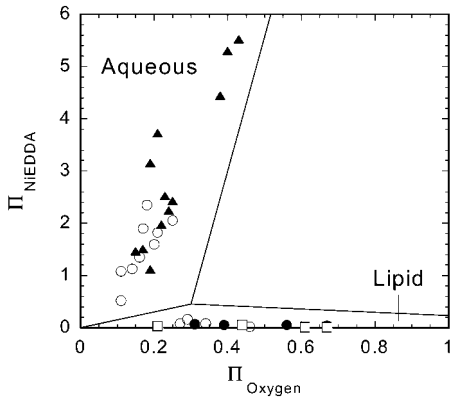

FIGURE 4: Collision data, Π^{oxy} versus Π^{NiEDDA}, for the R1 side chain attached to the C2 domain. Data points are shown for the C2 domain in aqueous solution (▲) and bound to PC/PS (3:1) membranes (○). Collision data are also shown for doxyl-labeled phospholipids (●) and spin-labeled bR mutants (□). The placement of boundaries indicating label environment was taken from data published for bacteriorhodopsin (*39*). For the C2 domain protein in the absence of lipid, all mutants are located in the aqueous region of the chart. In the presence of lipid, all C2 domain mutants are in the aqueous region, with the exception of 35, 39, 96, and 98, which are found in the lipid region. As expected, spin-labeled PCs and bR mutants are located in the lipid region of the chart.

the C2 domain in aqueous solution, the C2 domain bound to membranes, spin-labeled lipids incorporated into POPC/POPS membranes, and bacteriorhodopsin mutants. In the absence of membranes, the protein spin-labeled sites have collision parameters consistent with an aqueous exposure. When bound to POPC/POPS membranes, four of the labeled sites (35, 39, 96, and 98) have collision parameters that clearly place these residues within the lipid bilayer. Thus, the collision parameters correlate with the scaled spin label mobilities (Figure 3). It should be noted that R1 at position 64 does not penetrate the bilayer; however, it does have the lowest value of Π^{NiEDDA} for any of the labels with aqueous exposure and thus likely lies near the bilayer. As expected, spin-labeled lipids and bR mutants have Π values associated with the lipid region of Figure 4.

For each spin-labeled lipid or protein, the depth parameter, Φ, was determined from the collision parameters Π^{oxy} and Π^{NiEDDA} as summarized in Table 2. All of the Φ values for spin-labeled lipids and bR mutants are positive due to the high frequency of collision with oxygen, and a low frequency of collision with NiEDDA. By contrast, most of the Φ parameters for the membrane-bound C2 domain are highly negative, indicating aqueous exposure, except for the spin-labeled sites 35, 39, 96, and 98. These spin-labeled residues exhibit positive values of Φ, indicating that they penetrate the bilayer. Insertion of these residues indicates that the first and third Ca^{2+}-binding loops of the C2 domain reside within the membrane.

Modeling the Depth Dependence of Φ *and the Location of the Membrane-Bound C2 Domain.* To orient the C2 domain relative to the membrane, a procedure that simultaneously explored both the spatial dependence of Φ and the geometry of the protein−membrane complex was developed. This modeling utilized five types of constraints: (i) an equation describing the behavior of the depth parameter, Φ-(x); (ii) the experimental Φ values from the spin-labeled C2 domain; (iii) Φ values for lipid and bacteriorhodopsin spin labels at known values of x; (iv) the known NMR solution structure of the C2 domain; and (v) the orientations of the protein-bound spin labels.

As indicated above (Materials and Methods), a hyperbolic tangent function was employed (eq 4) to describe Φ(x)

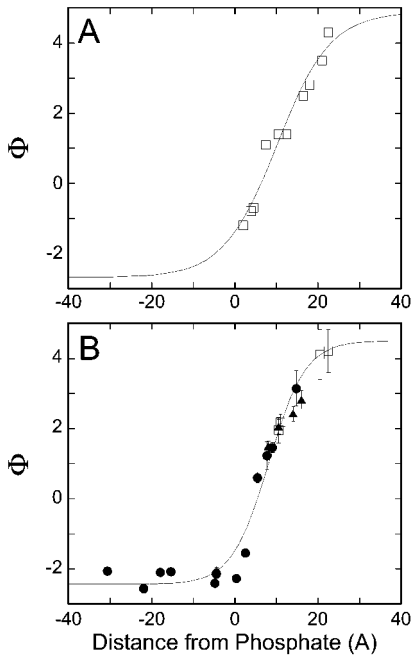

FIGURE 5: Calibration curves generated by computer simulations. (A) Previously measured bilayer depth parameters, Φ, plotted as a function of distance from the lipid phosphate for a series of spin-labeled bacteriorhodopsin mutants in egg-PC bilayers (*31*). These Φ parameters were measured using 20 mM nickel(II) acetylacetonate as the paramagnetic metal reagent. The solid line represents a fit of eq 4 to these data using an experimentally determined bulk aqueous value for Φ of −2.6 and an estimated Φ of 4.5 for the bulk hydrocarbon (parameters obtained from the fit are $A = 3.8$, $B = 0.079$, $C = 10.2$, and $D = 1.1$). (B) Depth parameter $\Phi(x)$ (solid line) determined by a fit of the measured Φ values for the C2 domain (●), doxyl-labeled phosphatidylcholines (▲), and bacteriorhodopsin mutants (□). The orientation and position of the domain along the bilayer normal were varied until a best, least-squares fit was obtained for the Φ parameters to eq 4 as described in the text. Values found for *A*, *B*, *C*, and *D* in eq 4 were 3.5, 0.11, 8.2, and 1.0, respectively.

because it exhibits the correct limiting behavior. To provide additional justification for this choice, eq 4 was tested on a previously published data set obtained for bacteriorhodopsin (*31*). Figure 5A illustrates a best-fit of this function to the data. This fit was constrained by the aqueous bulk limit, which is the difference $(D - A)$ in eq 4. This bulk limit was experimentally determined to be $\Phi = -2.6$ by measuring the Φ value for aqueous 3-carboxyproxyl. The limit in the membrane interior $(D + A)$ was estimated to be $\Phi = 4.5$ based on the maximal Φ values observed for deeply buried spin labels (*31*). Equation 4 clearly provides a reasonable fit to these data and has an approximately linear dependence inside the membrane with a smooth transition to the limiting aqueous value. It should be noted that while this empirical expression fits reasonably well with the existing data, additional data (particularly in the headgroup region) might ultimately indicate that a more complex function is required.

The data shown in Figure 5A were obtained using a different metal reagent and in membranes having a different composition than those used here. To define $\Phi(x)$ for the lipids and reagents used here, values of Φ were obtained for spin-labeled lipids and spin-labeled bR at known positions relative to the headgroup phosphate. Coordinates for the spin-labeled C2 domain mutants were generated as detailed under Materials and Methods. To fit the data to eq 4, three

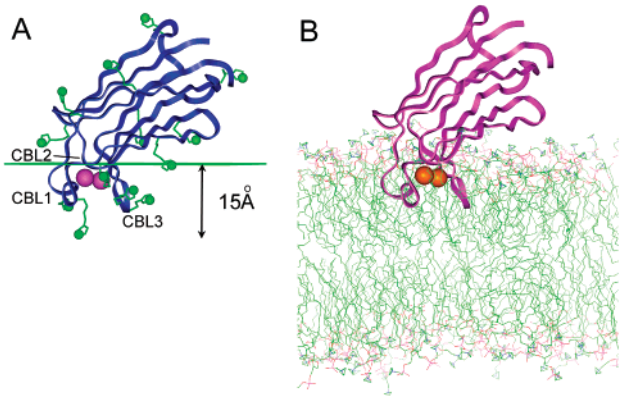

FIGURE 6: Orientation of the averaged NMR structure of the C2 domain on the membrane interface produced by the fit shown in Figure 5B. Both the first and third Ca^{2+}-binding loops are buried deeply within the bilayer. The backbone of the second Ca^{2+}-binding loop is positioned near the level of the lipid phosphates. (A) cPLA2 C2 domain (PDB ID: 1BCI) with MTSSL spin labels appended at 13 residues. The nitrogen in the nitroxide radical is depicted as a green sphere. Calcium ions are shown in magenta. The green plane that is illustrated is parallel to the bilayer interface and positioned at the level of the lipid phosphates. (B) Backbone rendering of the cPLA2 C2 domain (PDB ID: 1BCI) that is docked to a dynamically simulated POPC bilayer (*50*−*52*). Note that the bilayer structure was obtained from a dynamic simulation in the absence of protein.

parameters were simultaneously varied defining the shape of the hyperbolic tangent function ($D - A$, B, and C in eq 4), together with four parameters defining the angular orientation and depth of the spin-labeled C2 domain relative to the membrane surface. During this iterative process, the lipid and bacteriorhodopsin calibration points remained fixed. Ultimately the approach converged on a self-consistent model defining both the depth dependence of Φ and the position of the C2 domain on the membrane.

Figure 5B shows the experimental Φ values from the C2 domain and the best-fit membrane-associated depths along with the best-fit to eq 4. The best-fit suggests that the value of Φ reaches 95% of its bulk aqueous value at a distance of about 10 Å from the bilayer. In fact, the gradients change little at distances greater than 5 Å from the interface, making distance determinations by the collision-gradient method difficult beyond this point. Inside the membrane, Φ increases in an approximately linear fashion. The fit between eq 4 and the data is reasonably good, particularly given the assumptions made regarding spin label conformations and the possibility that the C2 domain structure may change upon membrane docking. The best-fit parameters defining $\Phi(x)$ (eq 4) were found to be the following: $A = 3.5$, $B = 0.11$, $C = 8.2$, and $D = 1.0$.

Orientation and Depth of the Membrane-Bound C2 Domain. Figure 6A, B illustrates the best-fit location of the C2 domain relative to the lipid phosphate layer at the membrane surface. The first and the third Ca^{2+}-binding loops are found at approximately the same distance within the membrane bilayer so that the backbones of these loops lie approximately 9−10 Å below the level of the lipid phosphates. At least one of the side chains attached to these loops rests considerably deeper in the interface due to the positioning of the backbone. For example, L39R1 resides at a position approximately 15 Å below the lipid phosphates. The backbone of the second Ca^{2+}-binding loop does not penetrate significantly into the membrane but is positioned near the

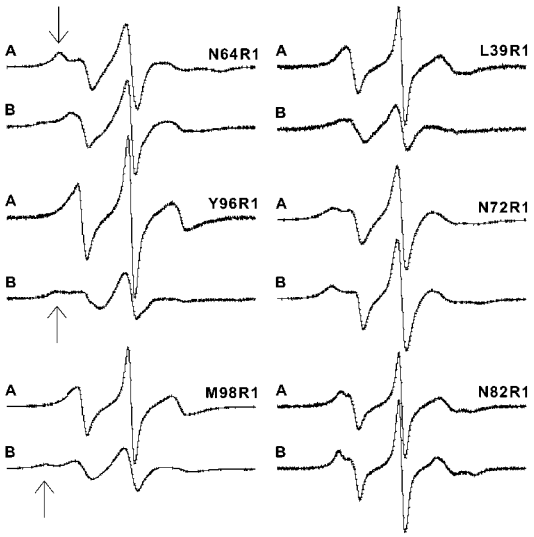

FIGURE 7: EPR spectra of several spin-labeled C2 domain sites (A) in aqueous solution in high-viscosity media and (B) in the presence of PC/PS membranes. In the presence of PC/PS membranes, the C2 domain is fully membrane-associated. In aqueous solution of sufficiently high viscosity, the rotational rate of the protein is slowed so that protein rotational diffusion does not significantly average the magnetic anisotropies that contribute to the EPR line shapes. Under these conditions, changes in line shape reflect changes due to differences in the interactions made by the R1 side chain. For the labels N64R1, Y96R1, and M98R1, arrows indicate broad components in the low-field resonance. These spectral components are a result of R1 that is undergoing tertiary contact within the protein or with immobilized lipid. The high-viscosity medium contained 30% Ficoll 400 in the standard EPR buffer (see Figure 2 legend).

level of the lipid phosphates such that some side chains on this loop could penetrate.[2] Strand 3 on the lower half of the β-sandwich is tilted upward at an angle of approximately 30° from the plane of the bilayer, while strand 5 (on the upper half of the β-sandwich) is positioned approximately 45° from the plane of the bilayer.

EPR Spectra Indicate Changes in Side-Chain Tertiary Contact upon Membrane Binding. To determine whether the changes seen between the aqueous and membrane-bound EPR spectra in Figure 2 were due entirely to changes in the rotational rate of the C2 domain, we acquired aqueous spectra in a high-viscosity medium. As discussed elsewhere, high viscosity slows the rotational diffusion of the protein in solution but does not significantly alter side chain dynamics (*40*). Under these conditions, EPR spectra reflect the local motion of the label, which should primarily be determined by rotations about the fourth and fifth dihedral angles of the side chain and by backbone dynamics (*38*).

Figure 7 shows a comparison between EPR spectra for the C2 domain in aqueous solution in a high-viscosity medium and bound to lipid bilayers. In all cases examined, the lipid-bound spectra were not influenced by the presence of a high-viscosity medium. At positions that are exposed to the aqueous phase in the membrane-docked state, for example, sites 59, 72, and 82, the spectra are similar and indicate that membrane docking immobilizes the domain without changing the local motion and interactions of the label. However, at sites that are near or within the membrane interior, sites 39, 64, 96, and 98, the solution and membrane-bound spectra are significantly different. At these sites, membrane docking not only immobilizes the domain but also alters the local motions of the R1 side chains at these positions. In the case of residue 39, the R1 side chain is localized deep within the bilayer, and the broadening is likely the result of an interaction of the side chain with the membrane hydrocarbon. For the R1 side chain at positions 96 and 98, a broad component appears in the low-field region upon membrane binding (see arrows in Figure 7), which is characteristic of R1 immobilization due to tertiary contact. This tertiary contact could be due to interactions with immobilized lipid or steric interactions that accompany structural changes in the Ca^{2+}-binding loops upon membrane docking. An opposite change takes place for the N64R1 label. In this case, tertiary contact that is seen in the aqueous phase is partially removed upon membrane docking of the C2 domain. The increase in motion is due to a change in the local environment of the label, and could reflect an altered conformation of the second Ca^{2+}-binding loop. In fact, modeling of the C2 domain suggests that an outward twist of this loop could account for the increased label mobility. It should be noted, however, that N64R1 is significantly perturbed in its membrane binding. In addition, molecular modeling indicates that R1 cannot be introduced in its preferred conformation into the solution structure of the C2 domain at site 64 (see Materials and Methods). As a result, R1 may not be well tolerated at this site, and the changes in motion may be unique to this label. Additional measurements will be required to determine whether there are indeed changes in the structure of this Ca^{2+}-binding loop upon membrane binding.

DISCUSSION

In the work described here, site-directed spin labeling was used to investigate the orientation and position of the C2 domain of cPLA2 on membrane surfaces. This was accomplished by using depth parameters (Φ) for known positions on the C2 domain, together with the known structure of the C2 domain and multiple calibration points to orient the domain at the membrane interface. Collision gradients for O_2 and metal ions through the bilayer are known to produce a roughly linear behavior of Φ within the bilayer interior (*31*, *41*). Although the exact shape of the dependence through the interface and outside the bilayer is not known, Φ must reach a limiting value in solution and in bulk hydrocarbon. We assumed a hyperbolic tangent shape for $\Phi(x)$ (eq 4) and simultaneously varied the steepness and width of this function, together with the orientation and depth of the C2 domain relative to the membrane, to develop a self-consistent model for the depth dependence of Φ and the geometry of the protein−membrane complex. In principle, any number of functions might have been used to describe $\Phi(x)$, but the choice of eq 4 is reasonable because it produces the correct limiting behavior in the bulk aqueous phase, yields a roughly linear region within the bilayer

[2] In Figure 6A, residue N64R1, in loop 2, appears to be located slightly within the bilayer interior. This is inconsistent with the collision data given in Table 2 and Figure 4, which localize the labeled side chain outside the bilayer. This discrepancy may be due in part to conformational differences between the membrane-bound form and the NMR solution structure, and to greater uncertainty in the configuration of the labeled side chain for position 64 due to steric constraints. As indicated by the data shown in Figure 7, there appears to be a change in the structure of N64R1 upon membrane binding.

interior, and approaches a maximum inside the bilayer. The shape of $\Phi(x)$ shown in Figure 5 indicates that the collision gradients do not change significantly at a distance more than 5 Å from the phosphate group on the aqueous side of the membrane interface. As a result of this dependence, distance errors rise significantly when Φ drops below a value of -2, such that the method does not accurately define distances more than a few angstroms off the membrane interface. This behavior for Φ is consistent with EPR measurements made on basic peptides that reside several angstroms from the membrane interface (*42*).

In addition to the intrinsic error in the measurement of Φ, there are several other sources of error that limit the accuracy of the fit shown in Figure 5 and hence the orientation and depth determined for the C2 domain. The membrane depths of the lipid nitroxide probes used to calibrate the protein data are not precisely known and could vary from the assumed values if these lipids undergo extensive conformational dynamics. Although we have made reasonable guesses regarding the conformation of R1, the orientations of the labeled side chains on the labeled domain are not precisely known. To test the sensitivity of the fit to side chain conformation, we varied the positions of several important side chains through a range of rotomeric states. Despite these changes, we still obtain reasonable fits that produce approximately the same membrane position for the domain as that shown in Figure 6 (data not shown). Another potential source of error is the assumption that the C2 domain solution structure does not change upon membrane binding. While small changes in the structure are possible, the reasonable fit shown in Figure 5B argues against drastic structural changes upon membrane binding. Previous NMR studies of the domain docking to micelles found that chemical shift changes were mainly localized to the calcium- and membrane-binding loops, and fluorescence studies found that the majority of probes perturbed by membrane docking were on or near the membrane-binding loops (*17*, *21*).

It is interesting to note that several labels lying within the aqueous phase exhibit depth parameters that differ significantly from one another, given the known experimental error. Because these labels are relatively distant from the interface, and because they are designed to be fully surface-accessible, they should all have values of Φ near that for a protein label in the bulk aqueous phase. This variation is consistent with recent work showing that there is a substantial variation in the O_2 enhancements of nuclear relaxation rates for fully surface-exposed residues on ribonuclease A (*43*). Such differences are thought to be steric in origin, resulting from differences in hydration or counterion density. Thus, some scatter in the fit shown in Figure 5B could arise from the effects of local structure and electrostatics on the collision rates between O_2 or NiEDDA and the R1 side chain. Improvement in the determination of this membrane-associated structure could be made with measurements on additional spin-labeled mutants and experiments that define the structural changes that occur upon membrane binding.

Several previous studies have been directed at determining the docking surface and orientation of this C2 domain on the membrane interface, and the position found here shows some similarities and interesting differences with previous work. The docking surface identified by fluorescence labeling of the same sites is in excellent agreement with the present results (*21*). In the fluorescence study, 5-FM probes located at the 35, 39, 96, and 98 positions were the most strongly perturbed by membrane binding, while a probe at position 64 displayed a weaker but detectable perturbation, and a probe at position 68 showed no detectable perturbation. This follows the pattern observed in Table 2 for the EPR collisional parameters of the same-labeled positions. The present EPR data indicate that the first and third Ca^{2+}-binding loops interact strongly with the bilayer, and that the second Ca^{2+}-binding loop interacts more weakly. This conclusion is generally consistent with the results of the lipid affinities measured by FRET as summarized in Table 1. The increase in membrane affinity upon incorporation of R1 at sites in the first and third Ca^{2+}-binding loops is consistent with a hydrophobic interaction between the spin label and the bilayer interior. Incorporation of R1 outside these loops has little effect on the membrane affinity.

A previous study based upon site-directed mutagenesis and monolayer studies implicated the same loops in membrane docking (*23*); however, the present EPR data position the first and third Ca^{2+}-binding loops substantially deeper within the bilayer interior. In an earlier EPR study, the domain was found to be tilted so that the backbone of β-strand 3 interacts with the membrane (*22*). No evidence was found here or in the previous fluorescence work for membrane contact of this β-strand. This earlier EPR study utilized a different approach than that used here and was carried out at lower ionic strength and in membranes composed entirely of acidic lipid. These conditions may have promoted a stronger electrostatic interaction between the basic cluster on β-strand 3 and the highly anionic membrane surface. Indeed, previous work carried out on basic peptides indicates that the position of charged residues above the membrane interface is dependent upon membrane surface charge density (*42*, *44*). The resulting C2 domain tilt found here still allows for an electrostatic interaction between β-strand 3 and the membrane interface. In fact, with the lipid composition and ionic strength used here, an optimal interaction between positively charged side chains and the anionic membrane surface is obtained when these charged residues lie several angstroms off the interface (*42*, *44*, *45*).

The new model presented here for the C2 domain−membrane interaction places the spin-labeled side chains of the first loop as deep as 15 Å below the lipid phosphates. The protein backbone is found as deep as 10 Å, near the lipid carbonyl and well removed from bulk water. As noted previously, the membrane docking of the cPLA2 C2 domain is driven primarily by hydrophobic interactions rather than by electrostatic interactions (*3*, *21*). The first and third Ca^{2+}-binding loops contain numerous hydrophobic side chains that could assist in the hydrophobic interactions between the protein and the bilayer, including F35, M38, L39, Y96, V97, and M98. Thus, the observation that these loops are deeply buried is fully consistent with the hydrophobic nature of the docking interaction. The penetration of the domain into the membrane places the Ca^{2+} ions near the carbonyl oxygens of the fatty acid ester linkages, which may replace the Ca^{2+}-coordinating water oxygens observed in the free domain. Alternatively, the domain may distort the local lipid structures so that Ca^{2+} coordination is provided by lipid phosphate oxygens as observed in the structure of the PKC-α C2 domain bound to a lipid analogue (*26*).

The present EPR results indicate that there may be changes in the structure of the C2 domain upon membrane binding. From the limited measurements made here, these changes could involve rearrangement of the first, second, and third Ca^{2+}-binding loops on the membrane-interacting face. Some of the spectral changes may be associated with interactions with immobilized phospholipids. If there are structural changes upon binding, they are likely to be quite minor, as suggested by the good fit obtained in Figure 5 using the solution NMR structure. Other studies have hinted at conformational changes within the C2 domain upon membrane binding (*28*, *34*), and, in particular, there is evidence for a rearrangement of the region near the second calcium-binding loop (*46*).

Several mechanisms might account for the Ca^{2+}-dependent membrane binding of this C2 domain. It has been proposed that Ca^{2+} neutralizes clusters of negative residues in the Ca^{2+}-binding loops, thereby reducing the desolvation and electrostatic penalties that would be experienced as the domain moves close to the membrane interface (*47*). The results obtained here demonstrate that the Ca^{2+}-binding loops penetrate deeply into the membrane interface; as a result, changes in dehydration energy in the loop regions upon Ca^{2+} binding would be an important factor in controlling the membrane association of this domain. Several sites within the membrane-interacting loop regions of the C2 domain show evidence for increases in label dynamics upon Ca^{2+} removal (*48*). This is not surprising since Ca^{2+} coordination would be expected to limit the conformations that could be assumed by the loops, thereby reducing their dynamics. The membrane-bound line widths of the C2 domain examined here indicate that labels on the membrane-docked loops are much less mobile than those on the opposite aqueous face of the protein. Although these observations need further investigation, they suggest that the conformational entropy of the backbone plays a role in the membrane binding of the cPLA2 C2 domain. Calcium may limit the flexibility of the loop regions so that they do not suffer an entropy loss that they might otherwise experience upon membrane binding. Finally, it has been proposed based upon crystallographic studies of the C2 domain from PLC-δ_1 that Ca^{2+} binding alters the exposure of hydrophobic residues in the loop region (*49*, *21*). The increased hydrophobicity of the membrane-interacting face might then facilitate the membrane interaction of the domain. At the present time, not enough is known about conformational differences that exist between the Ca^{2+}-bound and Ca^{2+}-free forms of the C2 domain from cPLA2 to evaluate this mechanism.

In summary, we used site-directed spin labeling to model the membrane depth and orientation of the cPLA2 C2 domain. The results indicate that the first and third Ca^{2+}-binding loops penetrate deeply into the bilayer, and that the second Ca^{2+}-binding loop interacts more weakly with the membrane surface. The EPR data also provide evidence that the structure of the C2 domain is subtly altered upon membrane binding, and that there are rearrangements in the Ca^{2+}-binding loop regions upon membrane association. Finally, we provide new information on the distance dependence of the depth parameter obtained from EPR collision gradient measurements. This distance dependence should prove useful in structural studies of other membrane-associated proteins.

ACKNOWLEDGMENT

We thank James D. Clark and the Genetics Institute for originally making available the expression system for cPLA2, and Duncan Greenhalgh and Gobind Khorana for making available the unfolded bacterioopsin mutants used in this work.

REFERENCES

1. McLaughlin, S., and Aderem, A. (1995) *Trends Biochem. Sci. 20*, 272−276.
2. Nalefski, E. A., and Falke, J. J. (1996) *Protein Sci. 5*, 2375−2390.
3. Nalefski, E. A., Wisner, M. A., Chen, J. Z., Sprang, S. R., Fukuda, M., Mikoshiba, K., and Falke, J. J. (2001) *Biochemistry 40*, 3089−3100.
4. Gibson, T. J., Hyvonen, M., Musacchio, A., Saraste, M., and Birney, E. (1994) *Trends Biochem. Sci. 19*, 349−353.
5. Coussens, L., Parker, P. J., Rhee, L., Yang-Feng, T. L., Chen, E., Waterfield, M. D., Francke, U., and Ullrich, A. (1986) *Science 233*, 859−866.
6. Knopf, J. L., Lee, M. H., Sultzman, L. A., Kriz, R. W., Loomis, C. R., Hewick, R. M., and Bell, R. M. (1986) *Cell 46*, 491−502.
7. Chapman, E. R., An, S., Edwardson, J. M., and Jahn, R. (1996) *J. Biol. Chem. 271*, 5844−5849.
8. Desai, R. C., Vyas, B., Earles, C. A., Littleton, J. T., Kowalchyck, J. A., Martin, T. F., and Chapman, E. R. (2000) *J. Cell Biol. 150*, 1125−1136.
9. Rizo, J., and Sudhof, T. C. (1998) *J. Biol. Chem. 273*, 15879−15882.
10. Evans, J. H., Spencer, D. M., Zweifach, A., and Leslie, C. C. (2001) *J. Biol. Chem.*, online.
11. Kramer, R. M., and Sharp, J. D. (1997) *FEBS Lett. 410*, 49−53.
12. Dessen, A. (2000) *Biochim. Biophys. Acta 1488*, 40−47.
13. Hirabayashi, T., and Shimizu, T. (2000) *Biochim. Biophys. Acta 1488*, 124−138.
14. Sutton, R. B., Davletoc, B. A., Berghuis, A. M., Sudhof, T. C., and Sprang, S. R. (1995) *Cell 80*, 929−938.
15. Essen, L. O., Perisic, P., Katan, M., and Williams, R. L. (1996) *Nature 380*, 595−602.
16. Pappa, H., Murray-Rust, J., Dekker, L. V., Parker, P. J., and McDonald, N. Q. (1998) *Structure 6*, 855−894.
17. Xu, G.-Y., McDonagh, T., Yu, H.-A., Nalefski, E. A., Clark, J. D., and Cumming, D. A. (1998) *J. Mol. Biol. 280*, 485−500.
18. Shao, X., Fernandez, I., Sudhof, T. C., and Rizo, J. (1998) *Biochemistry 37*, 16106−16115.
19. Perisic, O., Fong, S., Lynch, D. E., Bycroft, M., and Williams, R. L. (1998) *J. Biol. Chem. 273*, 2596−2604.
20. Sutton, R. B., Ernst, J. A., and Brunger, A. T. (1999) *J. Cell Biol. 147*, 589−598.
21. Nalefski, E. A., and Falke, J. J. (1998) *Biochemistry 37*, 17642−17650.
22. Ball, A., Nielsen, R., Gelb, M. H., and Robinson, B. H. (1999) *Proc. Natl. Acad. Sci. U.S.A. 96*, 6637−6642.
23. Bittova, L., Sumandea, M., and Cho, W. (1999) *J. Biol. Chem. 274*, 9665−9672.
24. Dessen, A., Tang, J., Schmidt, H., Stahl, M., Clark, J. D., Seehra, J., and Somers, W. S. (1999) *Cell 97*, 349−360.
25. Nalefski, E. A., McDonagh, T., Somers, W., Seehra, J., Falke, J. J., and Clark, J. D. (1998) *J. Biol. Chem. 273*, 1365−1372.
26. Verdaguer, N., Corbalan-Garcia, S., Ochoa, W. F., and Gomez-Fernandez, J. C. (1999) *EMBO J. 18*, 6329−6338.
27. Davletov, B., Perisic, O., and Williams, R. L. (1998) *J. Biol. Chem. 273*, 19093−19096.
28. Lichtenbergova, L., Yoon, E. T., and Cho, W. (1998) *Biochemistry 37*, 14128−14136.
29. Hubbell, W. L., Gross, A., Langen, R., and Lietzow, M. A. (1998) *Curr. Opin. Struct. Biol. 8*, 649−656.
30. Hubbell, W. L., Cafiso, D. S., and Altenbach, C. (2000) *Nat. Struct. Biol. 7*, 735−739.

31. Altenbach, C., Greenhalgh, D. A., Khorana, H. G., and Hubbell, W. L. (1994) *Proc. Natl. Acad. Sci. U.S.A. 91*, 1667−1671.
32. Altenbach, C., Flitsch, S. L., Khorana, H. G., and Hubbell, W. L. (1989) *Biochemistry 28*, 7806−7812.
33. Mchaourab, H., Lietzow, M., Hideg, K., and Hubbell, W. (1996) *Biochemistry 35*, 7692−7704.
34. Nalefski, E. A., Slazas, M. M., and Falke, J. J. (1997) *Biochemistry 36*, 12011−12018.
35. Farahbakhsh, Z. T., Altenbach, C., and Hubbell, W. L. (1992) *Photochem. Photobiol. 56*, 1019−1033.
36. Dalton, L. A., McIntyre, J. O., and Fleischer, S. (1987) *Biochemistry 26*, 2117−2130.
37. Langen, R., Oh, K. J., Cascio, D., and Hubbell, W. L. (2000) *Biochemistry 39*, 8396−8405.
38. Columbus, L., Kalai, T., Jeko, J., Hideg, K., and Hubbell, W. L. (2001) *Biochemistry 40*, 3828−3846.
39. Hubbell, W., and Altenbach, C. (1994) *Curr. Opin. Struct. Biol. 4*, 566−578.
40. Langen, R., Cai, K., Altenbach, C., Khorana, H. G., and Hubbell, W. L. (1999) *Biochemistry 38*, 7918−7924.
41. Qin, Z., and Cafiso, D. S. (1996) *Biochemistry 35*, 2917−2925.
42. Victor, K. G., and Cafiso, D. S. (2001) *Biophys. J. 81*, 2241−2250.
43. Teng, C.-L., and Bryant, R. G. (2000) *J. Am. Chem. Soc. 122*, 2667−2668.
44. Victor, K., Jacob, J., and Cafiso, D. S. (1999) *Biochemistry 38*, 12527−12536.
45. Ben-Tal, N., Honig, B., Peitzsch, R. M., Denisov, G., and McLaughlin, S. (1996) *Biophys. J. 71*, 561−575.
46. Perisic, O., Paterson, H. F., Mosedale, G., Lara-Gonzalez, S., and Williams, R. L. (1999) *J. Biol. Chem. 274*, 14979−14987.
47. Murray, D., McLaughlin, S., and Honig, B. (2000) *Biophys. J. 78*, 188A.
48. Frazier, A., Wisner, M., Falke, J., and Cafiso, D. (2000) *Biophys. J. 78*, 415A.
49. Grobler, J. A., Essen, L.-O., Williams, R. L., and Hurley, J. H. (1996) *Nat. Struct. Biol. 3*, 788−795.
50. Tieleman, D. P., Berendsen, H. J., and Sansom, M. S. (1999) *Biophys. J. 76*, 3186−3191.
51. Tieleman, D. P., Berendsen, H. J., and Sansom, M. S. (1999) *Biophys. J. 76*, 1757−1769.
52. Tieleman, D. P., Sansom, M. S., and Berendsen, H. J. (1999) *Biophys. J. 76*, 40−49.

BI0160821